Electrochimica Acta 367 (2021) 137469

Contents lists available at ScienceDirect

Electrochimica Acta

journal homepage: www.elsevier.com/locate/electacta

Pulse Reverse Protocol for efficient suppression of dendritic micro-structures in rechargeable batteries

Asghar Aryanfar[a,b,*], Yara Ghamlouche[a], William A. Goddard III[c]

[a] American University of Beirut, Riad El-Solh 1107, Lebanon
[b] Bahçeşehir University, 4 Çırağan Cad, Beşiktaş, Istanbul 34353, Turkey
[c] California Institute of Technology, 1200 E California Blvd, Pasadena, CA 91125, United States

ARTICLE INFO

Article history:
Received 25 September 2020
Revised 8 November 2020
Accepted 10 November 2020
Available online 19 November 2020

Keywords:
Pulse Reverse Charging
Dendritic Microstructures
Electro-deposition/dissolution

ABSTRACT

The ramified and stochastic evolution of dendritic microstructures has been a major issue on the safety and longevity of rechargeable batteries, particularly for the utilization metallic electrodes. We computationally develop pulse-reverse protocols for effective halting of the growing microstructures during extensive charging periods far beyond inter-ionic collisions. Our framework is based on the competitiveness of the dendritic growth during the pulse period versus the dissolution of the (sub)branches during the reverse charge. The detachment of the atoms from the structure preferentially occurs from the metastable sites which possess the lowest coordination number and require lowest activation energy for dissolution. We prove that even an infinitesimal pulse-reverse charge is more effective than an extended pulse-relaxation method for the suppression of the dendritic structures.

1. Introduction

Metallic anodes are arguably popular materials for their applicability in the future rechargeable batteries [1–3]. Specifically, lithium metal possesses the lowest mass density which provides a very high energy density. It additionally has the highest electropositivity ($E^0 = -3.04\,V$ vs SHE) making it suitable for high-power applications. ($\rho = 0.53\ g\,cm^{-3}$) [4,5]. However, the quick formation of microstructures during the charge period leads to a tree-like formation of microstructures with high surface to volume ratio [6] which occupy a large volume, can reach the counter-electrode and short the cell. As well, they could dissolve from their thinner necks during the discharge period. Such a formation-dissolution cycle is particularly prominent for the metal electrodes due to lack of diffusion into the inner layers, as opposed to depositing in the surface [7]. Previous studies have investigated various factors on dendritic formation such as current density [8], electrode surface roughness [9,10], impurities [11], solvent and electrolyte chemical composition [12], electrolyte concentration [13], utilization of powder electrodes [14] and adhesive polymers [15], temperature [16], guiding scaffolds [17,18], capillary pressure [19], cathode morphology [20] and mechanics [21,22]. Some of the conventional characterization techniques used include NMR [23] and MRI [24]. Other studies also have shown the necessity of stability of solid electrolyte interphase (i.e. SEI) layer for controlling the nucleation and growth of the branched medium [25,26].

Earlier model of the branched evolution have addressed the electric field and space charge as the main driving mechanism [27] for growth while the other models focused on ionic concentration causing the diffusion limited aggregation (DLA) [28–30]. Both mechanisms are part of the electrochemical potential [31,32], indicating that each could be dominant depending on the localizations of the electric potential or ionic concentration within the medium. Nevertheless, their interplay has been rarely explored, especially in continuum scale and realistic time intervals, matching scales of the experimental time and space.

The main cause of dendritic formation is the non-uniformity of electrode surface morphology at the atomic scale and the Brownian nature of ionic motion during electrodeposition. A surface sharpness provides a large electric field that attracts the ions as a sink. The other contributing factor is the closeness of the asperity to the counter electrode, where more deposition accelerate the growth rate.

Pulse method has recently proven to be an effective mechanism for suppression of the dendrites [33,34]. The concentration of ions in a given region is the results of the cooperative role of the mass flux into/out of the region, as well consumption of ions due to reduction reaction. While the reaction process is probable during the interaction with any kind of surface, the influx of ions is in fact highly manipulated via the sharp and large elec-

* Corresponding author at: American University of Beirut, Riad El-Solh 1107, Lebanon.
E-mail address: aryanfar@caltech.edu (A. Aryanfar).

https://doi.org/10.1016/j.electacta.2020.137469
0013-4686/

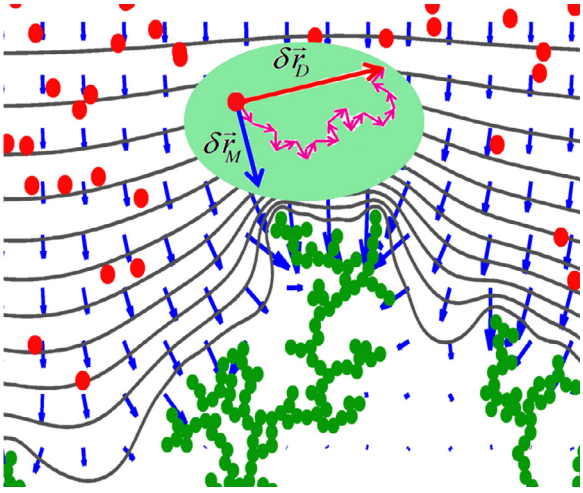

Fig. 1. The transport elements in the coarse scale of time.

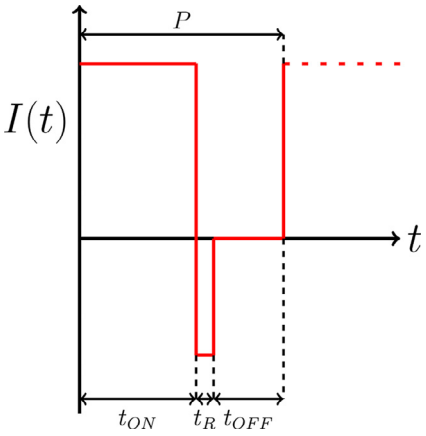

Fig. 2. Square pulse-reverse wave.

tric fields(i.e. $|\vec{E} \rightarrow 10^5\,\mathrm{V\,cm^{-1}}|$ [33]). Therefore during each pulse period, the ions unfavorably accumulate at the dendrites tips and during the subsequent rest period they favorably diffuse away to lower concentration zones. Such relaxation, which occurs within the double layer (or stern layer [35]), provides a useful mechanism to achieve uniform morphology. In fact, after the equilibrium, there is still ionic exchange between the above regions, with equal rates, due to Brownian motion, which occurs in local and global scales. Particularly, during higher charge rates, the ionic concentration is completely exhausted on the electrode surface [36]; Nevertheless, the continuum-level approach could extend to a larger scale, beyond the double layer region [37].

While the pulse-relaxation method reduces the evolution of the dendrites in batteries [33,38–40] and during other applications [41,42], the pulse-reverse method has specific advantages including saving the total charge time and retaining charge capacity. A pulse-reverse protocol consists of a positive pulse charge followed by a negative charge, with a possible optional resting time [43,44] as shown in the Fig. 2. This method reduces the concentration polarization [45] and is particularly used for controlling the thickness and uniformity of deposits [46]. With well chosen parameters, a larger cell' s specific energy and specific power can be reached with this technique [47,48]. Pulse-reverse is a potentially good method to overcome mass transport limitations in batteries [49]. This technique optimally decreases the possibly-formed concentration gradients. Therefore, the pulse-reverse has adequate potentials in terms of health and efficiency [43].

In this paper, we elaborate further in the range of acceptable reverse-ratio for suppression of stochastically-grown dendrites and we develop new insight for the effective rest period on the curved boundary. Subsequently we carry out experimental investigation to verify our analytical developments on the pulse parameters. We perform dimensional analysis to set our formulation applicable to the large range of electrochemical devices.

2. Methodology

The ionic motion is generated either from the variation of the concentration (∇C) or the electric potential ($\nabla\phi$). Typically, the ions in the high-concentrated zones collide and repel more and gradually move to less populated regions. In the larger scales such displacement can be represented by the diffusion length. On the other hand, ions tend to acquire drift velocity in the electrolyte medium when exposed to electric field. Therefore, as represented in the Fig. 1, the total displacement of the ions in the given coarse time interval of δt is given by[1]

$$\delta\vec{\mathbf{r}} = \sqrt{2D^{+}\delta t}\;\hat{\mathbf{g}} + \mu^{+}\vec{\mathbf{E}}\delta t \tag{1}$$

where D^+ is the ionic diffusion coefficient in the electrolyte, and $\hat{\mathbf{g}}$ is a normalized vector in a random direction, representing the Brownian dynamics, μ^+ is the mobility of cations in electrolyte, $\vec{\mathbf{E}}$ is the local electric field, which is the gradient of electric potential ($\vec{\mathbf{E}} = -\nabla\phi$).

The diffusion length represents the average progress of a diffusive wave in a given time, obtained directly from the diffusion equation. [50]

The pulse charging in its simplest form consists of trains of square active period t_{ON}, followed by a square rest interval t_{OFF} in terms of current I or voltage V as shown in Fig. 2. The period P is the time lapse of a full cycle defined as:

$$\begin{aligned} P &= t_{ON} + t_{REV} + t_{OFF} \\ &= t_{ON}(1 + f_{REV} + f_{OFF}) \end{aligned} \tag{2}$$

We define the reverse ratio f_{REV} as:

$$f_{REV} = \frac{t_{REV}}{t_{ON}} = \frac{Q_{REV}}{Q_{ON}} \tag{3}$$

which is solely true for the intended galvanostatic (i.e. constant current density) charging. In fact f_{REV} shows the fraction of the discharge-to-charge amount (i.e. $f_{REV} = 0.1$ means for every 10 attached atoms, there is 1 removal). As well we define the relaxation-ratio f_{OFF} as:

$$f_{OFF} = \frac{t_{OFF}}{t_{ON}} \tag{4}$$

Based on the Eqs. (2)–(4), the pulse reverse curve is uniquely characterized.

The reverse ratio f_{REV} is characterized based on charge amount whereas the relaxation-ratio f_{OFF} based on the amount of time. The algorithm defined in the Fig. 3 sets to enter the either. Hence, to enter the discharge phase, i.e. the reverse, a certain amount of charge needs to be met. This means that after a certain number of depositions, the program will set the phase to reverse and it will discharge the specified charge amount based on the reverse-ratio f_{REV}. In the ideal case, one can reduce the time to an infinitesimal amount and magnify the current i indefinitely. Therefore, the reverse phase could be explained as a Dirac delta function function below:

$$Q_{REV} = \lim_{t\to o}\int_0^t i.dt \tag{5}$$

[1] $\delta t = \sum_{i=1}^{n}\delta t_i$ where δt_k is the inter-collision time, typically in the range of fs.

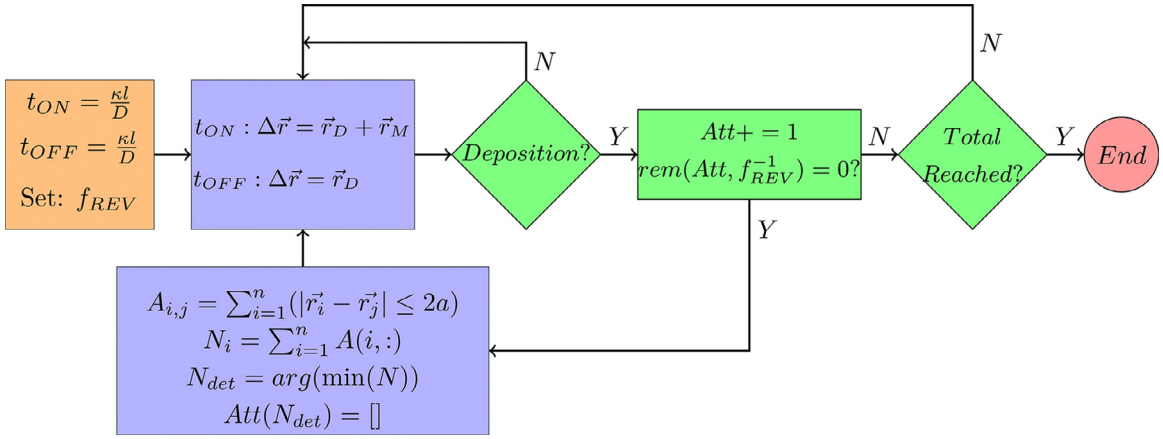

Fig. 3. Pulse-reverse pseudo-chart.

where the higher the current i is, the less time is needed to obtain the same discharge amount Q.

The electrodeposition-dissolution process for the formation of the dendritic morphologies is described in detail below:

1. Define the values for the time intervals composing the period P : they are the pulse period t_{ON}, rest period t_{OFF} and the reverse period t_{REV} which is defined through the reverse-ratio f_{REV}. The initial values are determined as the relaxation time scale for blocking electrodes, such that: [42]

$t_{on} = t_{off} = \frac{\kappa l}{D}$ where κ is the scale of the double-layer, l is the scale of the domain and D is the diffusivity coefficient of the bulk medium.

2. Determine the displacement of the each ion $\Delta\vec{\mathbf{r}}$ in the given time interval δt, where the pulse period carries the diffusion and migration effect, while the rest period only carries the sole diffusion effect. τ is the remainder of the total time divided by the period P and is the measure for determining the time zone, such that:

$$\tau := rem(t, P) \rightarrow \begin{cases} \tau \leq t_{ON} & \text{Pulse} \\ \tau > t_{ON} & \text{Relaxation} \end{cases}$$

3. Keep moving the ions, until (at least) one of them reaches the vicinity of dendrite and turns into the atom. If the program is in the charging phase, the atoms will both diffuse and attach to the structure. As long as the atoms are only diffusing, the loop keeps repeating itself. After each deposited atom, the program goes through a checkpoint. If the charge is divisible by $\frac{1}{f_{REV}}$, then the program will enter the reverse phase. Since $f_{REV} = \frac{t_{REV}}{t_{ON}}$ shows the fraction of time the discharge occurs relative to the charging period, therefore the term $rem(Att, f_{REV}^{-1}) == 0$ ensures entering into the detachment loop once every f_{REV}^{-1} times the attachment occurs. In the latter phase, the adjacency matrix $A_{i,j}$ of all the atoms will be calculated, which is a measure of the inter-atomic distance and $A_{i,j} = 1$ represents the two atoms being in the bond distance and 0 otherwise. The row sum leads to the number of neighbors for each atom.

4. In the reverse loop, the most metastable atom is removed. Thermodynamically such atom possesses the least coordination number (i.e. number of attached neighbors). Coordination number can be achieved by counting the number of atoms, which center-to-center distance of less than the atomic bond distance ($\sim 2a$) where $A_{i,j} = 1$. On the other hand, if the charge is not divisible by f_{REV}^{-1}, the loop is directed back to calculation of total time again unless the total number of atoms attached is reached. In the latter case, the program ends and the density of the atoms in the space filled is calculated and studied.

5. Continue step 1 to 4 until all desired number of atoms are attached (i.e. deposited).

Consequently, we define the density of the obtained microstructures as the filled-to-total fraction of the area as:

$\rho = \frac{n\pi r^2}{h_{max} l}$ where n is the number of atoms, r is the atomic radius, h_{max} is the height of the tallest atom and l is the scale of the domain. Fig. 5a and b represents the variation of the density ρ versus the reverse ratio f_{REV} and the relaxation ratio f_{OFF}.

Table 1
Experimental parameters.

Parameter	f_{REV}	i	l	R	T	C_∞
Value	{0, 0.2, 0.4, 0.6, 0.8}	1	3.175	7.95	298	1
Unit	[ ]	mA/cm^2	mm	mm	K	M

3. Experimental

We performed experiments within a manually-fabricated sandwich cell [51], which provides the possibility of *in-situ* observation of growing dendrites from the periphery (Fig. 6a). The cell encompasses two Li^0 disc electrodes ($D = 1.59$ cm) with the distance of $L = 0.32$ cm via a transparent acrylic PMMA separator. The fabricated cells were filled with 0.4 cm^3 of $LiPF_6$ in a solution with stoichiometric compound of EC:EMC≡1:1 in an argon-filled glovebox($H_2O, O_2 < 0.5$ ppm). Multiple such cells were electrolyzed with pulse reverse ratio values f_{REV} given in the Table 1, generated by a programmable multichannel cycler. After the passage of 48 mAh ($\approx$ 173 C) through the cells, 3 images within the periphery of 120^0 were taken by means of Leica M205FA optical microscope through the acrylic separator. The image processing algorithm is described as below:

1. The RGB image is read to the program by 3 values of $\{R, G, B\} \in [0, 255]$ and has been converted to a grayscale image I with individual values of range $I_{i,j} \in [0, 1]$.

2. The grayscale image $I_{i,j}$ is binarized to $J_{i,j}$via the grayness threshold I_c as below:

$$J_{i,j} = \begin{cases} 1 & I_{i,j} \geq I_c \\ 0 & I_{i,j} < I_c \end{cases}$$

the threshold value I_c has been chosen to minimize the weighted intra-class variance σ^2 defined as:

$$\begin{cases} \sigma^2 = \omega_0\sigma_0^2 + \omega_1\sigma_1^2 \\ \omega_0 + \omega_1 = 1 \end{cases}$$

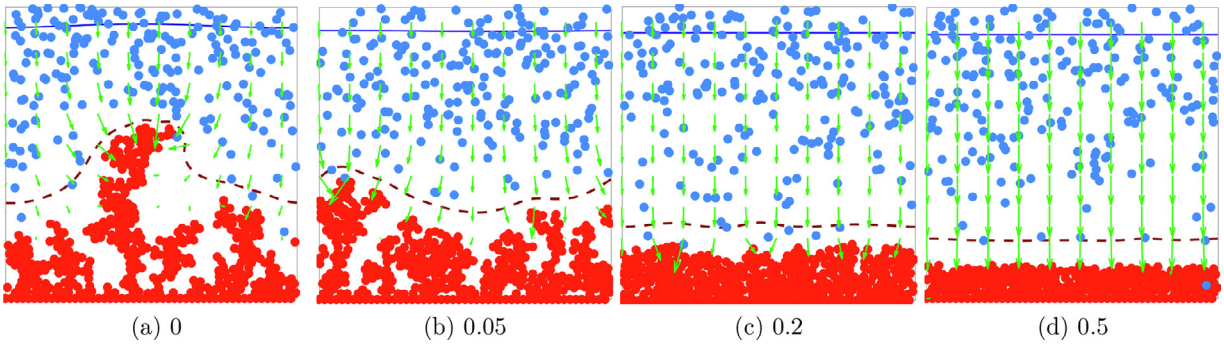

Fig. 4. Morphologies by the reverse ratio f_{REV}.

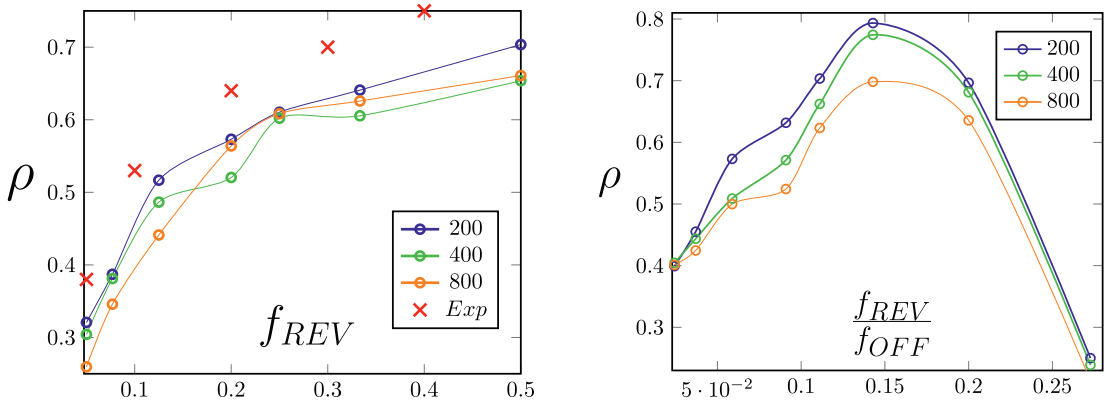

(a) Pulse-reverse ($t_{OFF} = 0$). (b) Pulse-reverse-relaxation ($t_{OFF} = \frac{\kappa l}{D}$).

Fig. 5. The density investigation versus pulse-reverse parameters. (For interpretation of the references to color in this figure, the reader is referred to the web version of this article.)

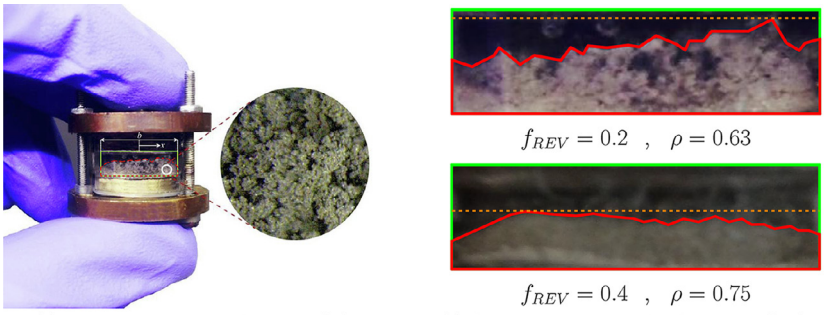

(a) Naked-eye observation of dendrites.[16] (b) Obtained morphologies for $f_{REV} = 0.2$ (top) and $f_{REV} = 0.4$ (bottom).

Fig. 6. Experimental procedure.

where ω_0 and ω_1 are the total fraction of element divided by the value of I_c and σ_0^2 and σ_1^2 are their respective variances. [52] Such minimization ensures that the resulted

3. The circular sandwich cell with the radius R has been divided of 3 arcs with the angle of $\frac{2\pi}{3}$ and width incremental length of δx, which is supposed to be projected to a 2D plane with the incremental width of $\delta x'$. From Fig. 6a due to geometry we have: $x = \frac{D}{2}\sin(\theta)$, $\rightarrow dx = \frac{D}{2}\cos(\theta)d\theta$, where $\cos(\theta) = \sqrt{1 - \frac{4x^2}{D^2}}$; hence:

$$\delta x' = \frac{\delta x}{\sqrt{1 - \frac{4x^2}{D^2}}}$$

where D is diameter of the sandwich cell [53].

4. Starting from the electrode surface, the occupied space by the dendrites has been calculated by the square site percolation paradigm [54].

5. The infinitesimal calculations have been integrated and normalized to inter-electrode distance ($\hat{\lambda}_i := \lambda_i / l$) to get the dendrite measure $\bar{\lambda}$ as:

$$\rho = \frac{1}{\pi D h_{max}} \sum_{k=1}^{3} \int_{-\frac{\pi}{3}}^{+\frac{\pi}{3}} \hat{\lambda}_k(\theta) \frac{D}{2} d\theta \qquad (6)$$

$$= \frac{1}{\pi D h_{max}} \sum_{k=1}^{3} \int_{-\frac{\pi}{3}}^{+\frac{\pi}{3}} \frac{\hat{\lambda}_k(x) dx}{\sqrt{1 - \frac{4x^2}{D^2}}}$$

where h_{max} is the height of the tallest peak in the observed dendrite. The integral Eq. (6) has been obtained by incremental sum

from experimental data. Fig. 6b shows such investigation for the sample reverse ratios of $f_{REV} = \{0.2, 0.4\}$, where the red encirclement is the approximated dendrite area, the green rectangle is the total area, and the dashed line represents the height of the tallest obtained dendrite in each experiment. The detailed experimental parameters are given in the Table 1.[2]

4. Results and discussions

During the excessive pulse period, which imposes the ionic flux on the dendrite body, the concentration order in the interface regions turns to the following due to manipulation from the electric field:

Concentration: $Tip > Bulk > Voids$ whereas, during a typical diffusion process, the flow of the ions occurs from high-to-low concentrated regions (i.e. $J = -D\nabla C$). Therefore, given enough time for the relaxation period, the concentration gradient should vanish, ensuring the equilibrium in ionic kinetics.

Fig. 4 shows that the reverse ratio f_{REV} correlates directly with the dendritic tendency. Starting from the uniform charging in the Fig. 4a the average height reduces consecutively through Fig. 4b–d where atoms leave the highly condensed sites and reattach on the inner unoccupied regions. This phenomenon is explained by the fact that the reverse current density at the tips is larger than in other locations which makes the high spots' atoms more prone to detachment [55] due to Arrhenius relationship as [56]:

$$k = k_0 \exp\left(-\frac{\Delta G}{k_B T}\right) \tag{7}$$

Therefore, due to lowest coordination number (i.e. $N = 1$), such sites require the lowest activation energy ΔG for dissolution and the preferential detachment of the high-spots with sharp interfaces leads to the melting of the peaks and the residue of smoother surface.

Fig. 5 a reveals that the density of the structures ρ versus the number of atoms increases with the reverse ratio f_{REV}, where each point is the average of the 3 individual runs. The increasing trend correlates with the previous studies that the reverse ratio is an effective method for dendritic suppression [49,57]. The experimental values correlated closely with the numerical simulations. The slight higher values of the experiments relative to the model can be interpreted as the result of the ignoring the void in the dendrites body (i.e. red encirclements) leading to the over-measurement in the experimental merit of density.

The density results in the Fig. 5b with identical reverse ratio f_{REV} are slightly higher in the presence of relaxation ratio f_{OFF}, which is additionally effective in vanishing the concentration gradients in the over-occupied zones until a certain limit. Nevertheless, the density decreases after a peak merging to smaller values by the reverse-ratio. The dissolution of the atoms is supposed to cut and shorten the branches in the structure and, in the best cases, completely remove them and flatten-out the interface. However, excessive dissolution will lead to the disturbing of the flat interface where the extra cavities form. Fig. 7 schematically explains such over-dissolution process, where the disruption occurs again. The green arrows indicate an increase in the $\frac{f_{REV}}{f_{OFF}}$ ratio and their intersection with the flat interface is at the critical value $\frac{f_{REV}}{f_{OFF}} \approx 0.15$.

The extended advantage of this the reverse-charing is the facilitation of the accessibility in ions to inner layer during the subsequent charge-discharge cycles. Comparing the Fig. 5a and b the cooperation of pulse-reverse (f_{REV}) and pulse-relaxation (f_{OFF}) is constructive, albeit pulse reverse shows much more efficacy for increasing the density. This has collectively been shown in the Fig. 8 where the relatively much smaller reverse ratio f_{REV} leads to much larger density values, even compared to extended relaxation ratio f_{OFF}. Thus, in order to reach comparable densities to the pulse-reverse technique, pulse-relaxation obliges a very long and unnecessary waiting time [49]. In practice, the partial discharge process can be imposed by programming the charger electronics and the entire pulse-reverse protocol could be automated to the infinitesimal (i.e. finite) time intervals, scaling down up to $\sim \mu$s. Needless to mention that, the results obtained are suitable and effective during a single charge period and short-term application, whereas the long term performance parameters such as coulombic efficiency and cycle stability will be studied in future works. Ultimately, tuning the morphology adjusts the distribution of the electric field and the concentration profile in the favor of uniform growth and since they are controlled not to reach extreme values, there will possibly be less side reactions.

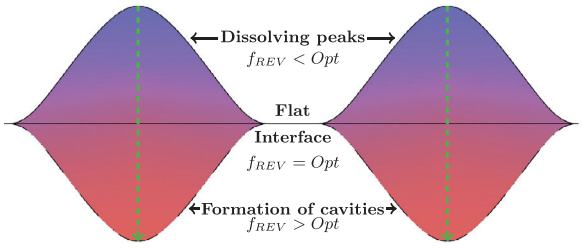

Fig. 7. The role of extreme reverse-ratio f_{REV} on the possible formation of cavities.

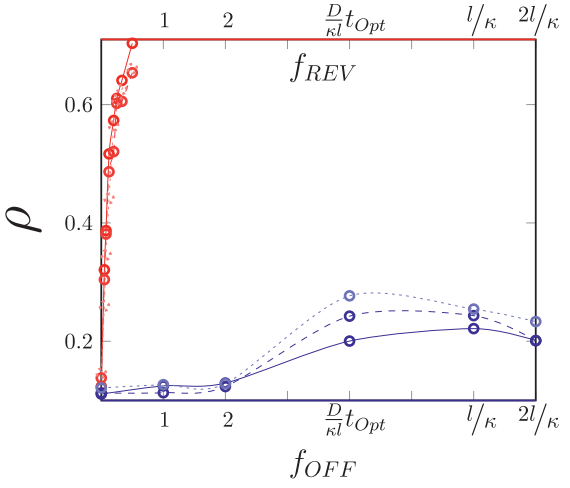

Fig. 8. Density values obtained via both imposing reverse-ratio f_{REV} (red) and the relaxation ratio f_{OFF} (blue). $\{Solid, Dashed, Dotted\} = \{200, 400, 800\}$atoms. (For interpretation of the references to color in this figure legend, the reader is referred to the web version of this article.)

5. Conclusion

In this paper, we have developed a reverse feedback control loop for more effective prevention of formation of dendritic growth during charge period of battery. The controlling parameters is mainly the charge-based reverse ratio f_{REV} accompanied with time-based relaxation ratio f_{OFF}. The preferential detachment of ions during the reverse charge correlates with the respective coordination number as well as their location in the microstruc-

[2] Note that the current density i and the ionic flux j are correlated with $i = zFj$, where z is the valence number of charge carriers and $F = 96.5$ kC/mol is the Faraday's constant, representing the amount of charge per mole.

ture. Both pulse-reverse and pulse-relaxation were investigated and compared with variant charge ratios. Pulse-reverse has shown to be the most efficient method for morphology control during dendritic evolution.

Declaration of Competing Interest

The authors declare that they have no known competing financial interests or personal relationships that could have appeared to influence the work reported in this paper.

Credit authorship contribution statement

Asghar Aryanfar: Conceptualization, Validation, Formal analysis, Investigation, Data curation, Writing - original draft, Writing - review & editing, Visualization, Funding acquisition. **Yara Ghamlouche:** Methodology, Resources, Software, Writing - review & editing, Supervision, Project administration. **William A. Goddard III:** Supervision, Project administration.

Acknowledgment

The authors would like to thank the University Research Board (URB) of American University of Beirut, Award #103950, for the financial support.

Supplementary material

Supplementary material associated with this article can be found, in the online version, at 10.1016/j.electacta.2020.137469.

References

[1] P. Pei, K. Wang, Z. Ma, Technologies for extending zinc air battery's cycle life: a review, Appl. Energy 128 (2014) 315–324.
[2] M.D. Slater, D. Kim, E. Lee, C.S. Johnson, Sodium-ion batteries, Adv. Funct. Mater. 23 (8) (2013) 947–958.
[3] Y. Li, H. Dai, Recent advances in zinc–air batteries, Chem. Soc. Rev. 43 (15) (2014) 5257–5275.
[4] S. Li, J. Yang, Y. Lu, Lithium metal anode, Encyclopedia of Inorganic and Bioinorganic Chemistry, Wiley online library, pp. 1–21.
[5] W. Xu, J.L. Wang, F. Ding, X.L. Chen, E. Nasybutin, Y.H. Zhang, J.G. Zhang, Lithium metal anodes for rechargeable batteries, Energy Environ. Sci. 7 (2) (2014) 513–537, doi:10.1039/c3ee40795k.
[6] S. Xiong, M. Regula, D. Wang, J. Song, Toward better lithium–sulfur batteries: functional non-aqueous liquid electrolytes, Electrochem. Energy Rev. 1 (3) (2018) 388–402.
[7] Z. Li, J. Huang, B. Yann Liaw, V. Metzler, J. Zhang, A review of lithium deposition in lithium-ion and lithium metal secondary batteries, J. Power Sour. 254 (2014) 168–182.
[8] R. Zhang, X.-B. Cheng, C.-Z. Zhao, H.-J. Peng, J.-L. Shi, J.-Q. Huang, J. Wang, F. Wei, Q. Zhang, Conductive nanostructured scaffolds render low local current density to inhibit lithium dendrite growth, Adv. Mater. 28 (11) (2016) 2155–2162.
[9] C.P. Nielsen, H. Bruus, Morphological Instability During Steady Electrodeposition at Overlimiting Currents, arXiv preprint arXiv:1505.07571(2015).
[10] P. Natsiavas, K. Weinberg, D. Rosato, M. Ortiz, Effect of prestress on the stability of electrode–electrolyte interfaces during charging in lithium batteries, J. Mech. Phys. Solids 95 (2016) 92–111.
[11] J. Steiger, D. Kramer, R. Monig, Mechanisms of dendritic growth investigated by in situ light microscopy during electrodeposition and dissolution of lithium, J. Power Sour. 261 (2014) 112–119, doi:10.1016/j.jpowsour.2014.03.029.
[12] R. Younesi, G.M. Veith, P. Johansson, K. Edstrm, T. Vegge, Lithium salts for advanced lithium batteries: Li-metal, Li-O_2, and Li-S, Energy Environ. Sci. 8 (7) (2015) 1905–1922.
[13] A. Teyssot, C. Belhomme, R. Bouchet, M. Rosso, S. Lascaud, M. Armand, Inter-electrode in situ concentration cartography in lithium/polymer electrolyte/lithium cells, J. Electroanal. Chem.y 584 (1) (2005) 70–74.
[14] I.W. Seong, C.H. Hong, B.K. Kim, W.Y. Yoon, The effects of current density and amount of discharge on dendrite formation in the lithium powder anode electrode, J. Power Sour. 178 (2) (2008) 769–773, doi:10.1016/j.jpowsour.2007.12.062.
[15] G. Stone, S. Mullin, A. Teran, D. Hallinan, A. Minor, A. Hexemer, N. Balsara, Resolution of the modulus versus adhesion dilemma in solid polymer electrolytes for rechargeable lithium metal batteries, J. Electrochem. Soc. 159 (3) (2012) A222–A227.
[16] A. Aryanfar, T. Cheng, A.J. Colussi, B.V. Merinov, W.A. Goddard III, M.R. Hoffmann, Annealing kinetics of electrodeposited lithium dendrites, J. Chem. Phys. 143 (13) (2015) 134701.
[17] Y. Yao, X. Zhao, A.A. Razzaq, Y. Gu, X. Yuan, R. Shah, Y. Lian, J. Lei, Q. Mu, Y. Ma, et al., Mosaic RGO layer on lithium metal anodes for effective mediation of lithium plating and stripping, J. Mater. Chem. A 7 (19) (2019) 12214–12224.
[18] J. Qian, Y. Li, M. Zhang, R. Luo, F. Wang, Y. Ye, Y. Xing, W. Li, W. Qu, L. Wang, et al., Protecting lithium/sodium metal anode with metal-organic framework based compact and robust shield, Nano Energy 60 (2019) 866–874.
[19] W. Deng, W. Zhu, X. Zhou, F. Zhao, Z. Liu, Regulating capillary pressure to achieve ultralow areal mass loading metallic lithium anodes, Energy Stor. Mater. 23 (2019) 693–700.
[20] A.W. Abboud, E.J. Dufek, B. Liaw, Implications of local current density variations on lithium plating affected by cathode particle size, J. Electrochem. Soc. 166 (4) (2019) A667–A669.
[21] C. Xu, Z. Ahmad, A. Aryanfar, V. Viswanathan, J.R. Greer, Enhanced strength and temperature dependence of mechanical properties of li at small scales and its implications for li metal anodes, Proc. Natl. Acad. Sci. 114 (1) (2017) 57–61.
[22] P. Wang, W. Qu, W.-L. Song, H. Chen, R. Chen, D. Fang, Electro-chemo-mechanical issues at the interfaces in solid-state lithium metal batteries, Adv. Funct. Mater. (2019) 1900950.
[23] R. Bhattacharyya, B. Key, H. Chen, A.S. Best, A.F. Hollenkamp, C.P. Grey, In situ NMR observation of the formation of metallic lithium microstructures in lithium batteries, Nat. Mater. 9 (6) (2010) 504.
[24] S. Chandrashekar, N.M. Trease, H.J. Chang, L.-S. Du, C.P. Grey, A. Jerschow, 7Li MRI of Li batteries reveals location of microstructural lithium, Nat. Mater. 11 (4) (2012) 311–315.
[25] Y. Li, Y. Qi, Energy landscape of the charge transfer reaction at the complex Li/SEI/electrolyte interface, Energy Environ. Sci. 12 (4) (2019) 1286–1295.
[26] L.M. Kasmaee, A. Aryanfar, Z. Chikneyan, M.R. Hoffmann, A.J. Colussi, Lithium batteries: improving solid-electrolyte interphases via underpotential solvent electropolymerization, Chem. Phys. Lett. 661 (2016) 65–69.
[27] J.N. Chazalviel, Electrochemical aspects of the generation of ramified metallic electrodeposits, Phys. Rev. A 42 (12) (1990) 7355–7367.
[28] T.A. Witten, L.M. Sander, Diffusion-limited aggregation, Phys. Rev. B 27 (9) (1983) 5686.
[29] X. Zhang, Q.J. Wang, K.L. Harrison, K. Jungjohann, B.L. Boyce, S.A. Roberts, P.M. Attia, S.J. Harris, Rethinking how external pressure can suppress dendrites in lithium metal batteries, J. Electrochem. Soc. 166 (15) (2019) A3639–A3652.
[30] S. Douezan, F. Brochard-Wyart, Active diffusion-limited aggregation of cells, Soft Matter 8 (3) (2012) 784–788.
[31] D. Tewari, P.P. Mukherjee, Mechanistic understanding of electrochemical plating and stripping of metal electrodes, J. Mater. Chem. A 7 (9) (2019) 4668–4688.
[32] A.J. Bard, L.R. Faulkner, et al., Fundamentals and applications, Electrochem. Methods 2 (482) (2001) 580–632.
[33] A. Aryanfar, D. Brooks, B.V. Merinov, W.A. Goddard Iii, A.J. Colussi, M.R. Hoffmann, Dynamics of lithium dendrite growth and inhibition: pulse charging experiments and Monte Carlo calculations, J. Phys. Chem. Lett. 5 (10) (2014) 1721–1726.
[34] M.Z. Mayers, J.W. Kaminski, T.F. Miller III, Suppression of dendrite formation via pulse charging in rechargeable lithium metal batteries, J. Phys. Chem. C 116 (50) (2012) 26214–26221.
[35] M.Z. Bazant, B.D. Storey, A.A. Kornyshev, Double layer in ionic liquids: overscreening versus crowding, Phys. Rev. Lett. 106 (4) (2011) 046102.
[36] V. Fleury, Branched fractal patterns in non-equilibrium electrochemical deposition from oscillatory nucleation and growth, Nature 390 (6656) (1997) 145–148, doi:10.1038/36522.
[37] A. Aryanfar, D.J. Brooks, T. Cheng, B.V. Merinov, W.A. Goddard, A.J. Colussi, M.R. Hoffmann, Three dimensional modeling of dendrite growth in rechargeable lithium metal batteries, in: Meeting Abstracts, 15, The Electrochemical Society, 2015, p. 1154. –1154.
[38] A. Aryanfar, D.J. Brooks, W.A. Goddard, Theoretical pulse charge for the optimal inhibition of growing dendrites, MRS Adv. 3 (22) (2018) 1201–1207.
[39] A. Aryanfar, M.R. Hoffmann, W.A. Goddard III, Finite-pulse waves for efficient suppression of evolving mesoscale dendrites in rechargeable batteries, Phys. Rev. E 100 (4) (2019) 042801.
[40] H.Z.Z. Beh, G.A. Covic, J.T. Boys, Effects of pulse and dc charging on lithium iron phosphate (lifepo 4) batteries, in: Proceedings of the 2013 IEEE Energy Conversion Congress and Exposition, IEEE, 2013, pp. 315–320.
[41] M.S. Chandrasekar, M. Pushpavanam, Pulse and pulse reverse plating – conceptual, advantages and applications, Electrochim. Acta 53 (8) (2008) 3313–3322, doi:10.1016/j.electacta.2007.11.054.
[42] M.Z. Bazant, K. Thornton, A. Ajdari, Diffuse-charge dynamics in electrochemical systems, Phys. Rev. E 70 (2) (2004), doi:10.1103/PhysRevE.70.021506.
[43] F. Savoye, P. Venet, M. Millet, J. Groot, Impact of periodic current pulses on li-ion battery performance, IEEE Trans. Ind. Electron. 59 (9) (2011) 3481–3488.
[44] S.H. Lee, H. Lee, M.S. Cho, J.-D. Nam, Y. Lee, Morphology and composition control of manganese oxide by the pulse reverse electrodeposition technique for high performance supercapacitors, J. Mater. Chem. A 1 (46) (2013) 14606–14611.
[45] W. Cheng, W. Ge, Q. Yang, X. Qu, Study on the corrosion properties of nanocrystalline nickel electrodepositied by reverse pulse current, Appl. Surf. Sci. 276 (2013) 604–608.
[46] U. Landau, Periodic reverse plating for effective leveling, Extended Abstract n 615, The Electrochem Soc Extended Abstracts 93 (1993) 1.

[47] C.-F. Chiasserini, R.R. Rao, Pulsed battery discharge in communication devices, in: Proceedings of the 5th Annual ACM/IEEE International Conference on Mobile Computing and Networking, 1999, pp. 88–95.
[48] B. Shrestha, D.A. Wetz, P.M. Novak, Pulsed elevated rate discharge of electrochemical energy storage devices, IEEE Trans. Plasma Sci. 40 (10) (2012) 2462–2469.
[49] H. Yang, E.O. Fey, B.D. Trimm, N. Dimitrov, M.S. Whittingham, Effects of pulse plating on lithium electrodeposition, morphology and cycling efficiency, J. Power Sour. 272 (2014) 900–908.
[50] J. Philibert, One and a half century of diffusion: Fick, Einstein, before and beyond, Diffusion Fundam. 4 (6) (2006) 1–19.
[51] A. Aryanfar, Method and Device for Dendrite Research and Discovery in Batteries, 2017, (????). US Patent 9,620,808.
[52] N. Otsu, A threshold selection method from gray-level histograms, Automatica 11 (285-296) (1975) 23–27.
[53] A. Aryanfar, D.J. Brooks, A.J. Colussi, M.R. Hoffmann, Quantifying the dependence of dead lithium losses on the cycling period in lithium metal batteries, Phys. Chem. Chem. Phys. 16 (45) (2014) 24965–24970.
[54] A. Aryanfar, W. Goddard III, J. Marian, Constriction percolation model for coupled diffusion-reaction corrosion of zirconium in PWR, Corros. Sci. 158 (2019) 108058.
[55] W. Jiang, S.S. Sundarram, W. Li, Fabrication of microcellular metal foams with sphere template electrodeposition, Manuf. Lett. 2 (4) (2014) 118–121.
[56] S. Arrhenius, Über die dissociationswärme und den einfluss der temperatur auf den dissociationsgrad der elektrolyte, Z. Phys. Chem. 4 (1) (1889) 96–116.
[57] N. Hasani, M. Ghaemi, M. Javankbakht, Using Pulse-and Reverse Pulse Currents in Synthesis of Cathode Materials for Rechargeable Lithium-Ion Batteries (2013).